Focusing of an inertia-gravity wave packet by a baroclinic shear flow

N.R. Edwards* & C. Staquet

LEGI, Grenoble, France

August 27, 2004

To appear in *Dynamics of Atmospheres and Oceans*

Abstract

We investigate the interaction of a small-amplitude internal gravity wave packet in a rotating fluid with a baroclinic shear flow. Ray equations and three-dimensional direct numerical simulations of the Boussinesq equations are solved for this purpose. The shear flow has a simple structure and depends separately on the vertical and horizontal coordinates. We focus on the situation where the intrinsic frequency Ω of the wave packet increases as the packet propagates into the shear flow, due to the horizontal dependence of this flow. The packet is trapped in the neighbourhood of the $\Omega = N$ surface (where N is the spatially varying Brunt-Väisälä frequency) and the wave-induced velocity, which first decays because of dispersion, is amplified there. The ray equations show that the packet may undergo multiple reflections within a wave guide formed by sections of the $\Omega = N$ surface, and thus penetrate into the shear flow. Three-dimensional numerical simulations of the same problem show that most of the wave packet is actually dissipated once trapped because both the group velocity and the horizontal scale of the packet have strongly decreased through the interaction. Consequently, the wave packet is not able to travel across the shear flow, except when the latter vanishes locally.

*Present address: Climate and Environmental Physics, Physics Institute, University of Bern, Sidlerstrasse 5, CH-3012 Bern, Switzerland.

1 Introduction

The purpose of this paper is to investigate how inertia-gravity waves, which are internal gravity waves modified by rotation, may interact with a baroclinic shear flow, namely a horizontal flow with both a horizontal and a vertical shear. Such interactions occur generically in geophysical flows, as soon as inertia-gravity waves propagate in a wind or a current or encounter a vortical motion such as a large-scale vortex. The basic interaction mechanism is elementary: the wave is refracted by the ambient flow. The key point is that the interaction may result in energy exchange between the wave and the ambient flow at the levels where the intrinsic wave frequency reaches limiting values, so that the ambient flow is locally accelerated or decelerated. At those levels, the linear wave equation is either singular or degenerate (Jones 1967 [11]).

Theoretical approaches to this problem are linear (*e.g.* Booker & Bretherton 1967 [2], Ivanov & Morozov 1974 [10]) or weakly nonlinear (*e.g.* Brown & Stewartson 1982 [5]) and the WKB approximation is usually employed as a first step to deal with the complexity of the interaction (*e.g.* Bretherton 1966 [4], Olbers 1981 [17], Badulin & Shrira 1993 [1]).

A classical interaction problem is that of a wave propagating upward into a vertically sheared horizontal wind $U(z)$; the medium is stably stratified with constant Brunt-Väisälä frequency N_0 and the shear flow is stable (that is, the Richardson number $Ri = N_0^2/(dU/dz)^2$ is greater than $1/4$ everywhere). In this situation, the intrinsic wave frequency Ω decreases (in absolute value) as the wave packet propagates upward. The intrinsic frequency is the frequency measured in a frame of reference attached to the ambient flow in which the wave propagates. The linear theory in the WKB approximation was used by Bretherton (1966) [4] to investigate the interaction process. This approximation was relaxed by Booker & Bretherton (1967) [2], permitting them to show that a monochromatic wave is absorbed by the current at the singular level where the wave phase speed along the wind matches the wind velocity (the intrinsic frequency being zero at this level).

This work was extended by Jones (1967) [11] to a rotating fluid. The intrinsic frequency of the waves is now bounded below by the Coriolis frequency f (that is $f \leq |\Omega| \leq N$) and two singular levels arise where $\Omega = \pm f$. Jones showed that the behaviour of the waves is very similar to that in the non-rotating case, the monochromatic wave being absorbed at the $\Omega = \pm f$ levels. The work by Wurtele *et al.* (1996) [22] details the linear and nonlinear behaviour of a monochromatic wave as it approaches these singular levels, when the wave is continuously emitted from a source at $t = 0$: as long as the wave has not reached a steady state, it crosses the $\Omega = \pm f$ levels and its amplitude decreases exponentially near the $\Omega = 0$ critical level; the wave is therefore evanescent there. As time elapses, the wave reaches a steady state and is then absorbed at the singular levels. If nonlinear effects are important, the wave breaks near the singular levels while being

partly reflected. All these results closely match the description made for the non-rotating case in the neighbourhood of the $\Omega = 0$ critical level by Booker & Bretherton [2] and by *e.g.* Winters & D'Asaro (1994) [21] using three-dimensional numerical simulations.

Jones (1968) [12] also extended Booker & Bretherton's work to a potentially unstable shear flow, where the Richardson number is smaller than 1/4 somewhere in the fluid. Jones [12] thus showed that when the wave propagates upward such that the intrinsic frequency increases (in absolute value), over-reflection is possible at the levels where $\Omega = \pm N$, that is, the reflection coefficient may be greater than 1 (for $Ri > 1/4$, normal reflection occurs at the $\Omega = \pm N$ levels, that is the reflection coefficient is equal to 1).

In summary, for a vertical shear flow $U(z)$ in a non-rotating medium, in the linear theory, the wave is absorbed when $\Omega \to 0$ and reflected when $\Omega \to \pm N$ (over-reflection may occur if the shear flow is unstable to Kelvin-Helmholtz instability). When the medium is rotating, the absorbing levels correspond to $\Omega = \pm f$.

What happens when a monochromatic wave propagates into a horizontal shear flow $U(y)$ in a rotating medium with uniform stratification? When propagation occurs so that $|\Omega|$ *decreases*, the wave behaviour depends upon the stability of the shear flow: when the shear flow is inertially stable, the wave is always reflected, possibly with a transmitted component. When the shear flow is inertially unstable, over-reflection may occur (Öllers *et al.* 2003 [18]). Note the analogy between the latter behaviour and that found by Jones (1968) [12] for an unstable vertical shear flow. When the monochromatic wave propagates so that $|\Omega|$ *increases*, it is trapped in the neighbourhood of vertical planes defined by $\Omega = \pm N$. The mean flow is decelerated by the interaction in this case *i.e.* the wave-induced energy locally increases; the wave may then break in the neighbourhood of the $\Omega = \pm N$ trapping planes, as shown by Staquet & Huerre (2002) [19].

These situations are thus rather complex but still remain academic in the sense that the shear flow varies along one direction and the Brunt-Väisälä frequency of the background medium is constant. The interaction of a wave with a baroclinic shear flow of the form $U(y, z)$ has been addressed by only a few studies, some theoretical (Jones 1969 [13], Olbers 1981 [17], Badulin & Shrira 1993 [1]) and one experimental (Moulin & Flor 2004 [16]). The theoretical studies [13], [17] and [1] rely upon the linear theory in the WKB approximation. Olbers thus computed the solutions for a wave field interacting with a balanced (thermal wind) state whose isopycnals have a non-zero constant slope. Olbers found that the waves may be guided between the $\Omega = f$ and $\Omega = N$ planes (assuming $\Omega > 0$) and that a singular level of a very special kind exists within this guide: this level is transparent for waves propagating from one side while approaching from the other side results in critical-layer absorption.

The general behaviour of a wave propagating in a shear flow which varies both along y and z is therefore not obvious when, for instance, $|\Omega|$ increases during the wave propagation: the wave should be trapped with respect to the horizontal dependence of the shear flow but should be reflected with respect to the vertical dependence. What is the actual behaviour?

Our purpose is to investigate this question in a simple context. We rely on WKB theory to explore the parameter range and get some hints about the wave behaviour, and also perform three-dimensional nonlinear direct numerical simulations (DNS). The geophysical motivation of this work is to investigate whether wave-induced momentum transport can occur across the shear flow. In the present paper, we explore the wave behaviour as it propagates toward the current and qualitatively discuss the effect, if any, of the interaction on the current.

The physical model of the interacting wave packet and shear flow is described in the next section. This model is used as the initial condition of the Boussinesq equations, which are recalled in section 3 along with the numerical method to solve them. The ray equations are briefly presented in section 4 along with the numerical algorithm we employ to solve these equations. Results are presented in section 5 and conclusions are drawn in section 6.

2 Physical model

The problem we model numerically consists of an inertia-gravity wave packet propagating toward and interacting with a baroclinic shear flow. The purpose of this section is to specify these two fields.

2.1 The baroclinic shear flow (U(y,z), B(y,z))

Let (x, y, z), with z directed upwards, be a Cartesian coordinate system in the rotating reference frame attached to the fluid container (this container is the numerical domain in the present case or the tank of a laboratory experiment). The velocity field is denoted $\mathbf{u} = (u, v, w)$. The baroclinic shear flow consists of a velocity field along the x-direction $\mathbf{U}(y, z)$ in thermal wind balance with a buoyancy field $B(y, z)$:

$$f\frac{\partial U}{\partial z} = -\frac{\partial B}{\partial y}. \tag{1}$$

The baroclinic current is a horizontal shear layer with a vertical shear

$$\frac{U}{U_0} = \left[1 + \tanh\left(\frac{y - y_s}{L_s}\right)\right]\left[1 + \beta \sin\left(\frac{2\pi z}{H_s}\right)\right] - 1; \tag{2}$$

U_0 is the velocity scale ($-U_0$ is the speed when $y \to -\infty$), y_s is the horizontal location of the shear layer centre and L_s is the vorticity thickness. This initial condition implies that a wave

packet propagating from a region where $y \ll y_s$ travels, as y increases, from a medium translating uniformly along the x direction with speed $-U_0$, to a moving medium with both a vertical and a horizontal velocity shear. The parameter β represents the strength of the baroclinicity and H_s is the typical scale of the vertical shear. The shear flow becomes barotropic as β approaches zero. When $\beta = 1$, U and its first order partial derivatives vanish at planes $z = z_n$ defined by $\sin(2\pi z_n/H_s) = -1$, that is $z_n/H_s = -1/4 + n$ for any relative integer n. This case is discussed in section 5.4. For $\beta < 1$, $\partial U/\partial z$ vanishes at those planes because it changes sign while $|U|$ and $|\partial U/\partial y|$ take a minimum non-zero value there.

Let $B(y,z) + b'(x,y,z,t)$ denote the total buoyancy field, where $b'(x,y,z,t)$ refers to the deviation from the balanced field $B(y,z)$. At $t = 0$, b' is the buoyancy field of the wave packet. We introduce the Brunt-Väisälä frequency of the balanced state N defined as $N^2 = \partial B/\partial z$. The buoyancy field B is obtained by integrating the thermal wind relation (1):

$$B(y,z) = B_0(z) - fU_0 \frac{2\pi\beta}{H_s} \cos\left(\frac{2\pi z}{H_s}\right) \left[y - y_s + L_s \log\left(\cosh\left(\frac{y-y_s}{L_s}\right)\right)\right]. \tag{3}$$

$B_0(z)$ is the buoyancy field of the rest state, assumed to be linear. We also define the Brunt-Väisälä frequency of the rest state N_0 by $N_0^2 = \frac{dB_0}{dz}$. N_0 will be used as the frequency scale hereafter, so that the time scale will be N_0^{-1}.

It is important for the purpose of our study that the baroclinic shear flow is not subject to an intrinsic instability during the interaction with the wave. Let us examine which instabilities may occur and whether the shear flow is stable against them. The incoming wave packet would act as the perturbation. In the horizontal plane, the shear flow is inertially unstable if $f(f - \partial U/\partial y) < 0$. We chose the sign of U_0 (< 0) and f (> 0) such that this condition is not satisfied; of course, this does not garantee that the instability will not develop. The shear flow may also be unstable to Kelvin-Helmholtz instability. This instability has a maximum growth rate for a wavelength along the x direction of order $7L_s$ (*e.g.* Michalke 1964 [15]). Hence, this instability will grow for run 1 but the growth rate is so slow that the wave-shear flow interaction will not be modified over the duration we consider. The same analysis can be used to ensure that, whatever the run, no Kelvin-Helmholtz instability will appreciably grow due to the vertical shear of the current (note that the latter instability will also be opposed by the stable stratification).

2.2 The inertia-gravity wave packet

Let $\mathbf{k} = (k_x, k_y, k_z)$ refer to the main wave vector of an inertia-gravity wave packet and $\Omega = \Omega(\mathbf{k})$ to the associated intrinsic frequency. We recall the dispersion relation relating $\mathbf{k}$ and Ω for a

monochromatic wave in a fluid at rest (*e.g.* Leblond & Mysak 1978 [14]):

$$\Omega^2 = N^2 \frac{k_H^2}{k^2} + f^2 \frac{k_z^2}{k^2}, \tag{4}$$

which can also be written as

$$\frac{k_H^2}{k_z^2} = \frac{\Omega^2 - f^2}{N^2 - \Omega^2}; \tag{5}$$

$k_H = |\mathbf{k}_\mathrm{H}|$ denotes the modulus of the horizontal wave vector $\mathbf{k}_\mathrm{H} = (k_x, k_y)$ and $k = |\mathbf{k}|$. We assume that $\Omega > 0$ in the following.

Let s denote the steepness of the wave, defined such that isopycnals are locally vertical for $s = 1$ and overturned for $s > 1$. The steepness may be defined as

$$s = \frac{u'_{max}}{c_x}, \tag{6}$$

which is the ratio of the wave-induced velocity along the x direction to the phase velocity along that direction.

At initial time $t = 0$, we assume that the wave energy is localized about the line $y = y_p,\ z = z_p$ and confined within a wave packet of length L_p along y and height H_p along z. The steepness of the wave packet at $t = 0$ is thus of the form

$$s = s_0 \exp\left\{ -\left(\frac{y - y_p}{L_p}\right)^2 - \left(\frac{z - z_p}{H_p}\right)^2 \right\}, \tag{7}$$

where s_0 is the steepness at the packet centre.

Finally, we recall the polarization relations for a monochromatic inertia-gravity wave of steepness s (see *e.g.* Gill 1985 [9], Olbers 1981 [17]). These relations will be useful in section 4.2 below. Let (u', v', w', b') be the components of the wave-induced velocity and buoyancy fields and $\Phi = k_x x + k_y y + k_z z - \omega t$ the phase of the wave. The polarization relations are:

$$u' = s\left(\frac{\Omega k_x}{k_H^2} + I\frac{f k_y}{k_H^2}\right) e^{I\Phi} \tag{8}$$

$$v' = s\left(\frac{\Omega k_y}{k_H^2} - I\frac{f k_x}{k_H^2}\right) e^{I\Phi} \tag{9}$$

$$w' = -s\frac{\Omega}{k_z} e^{I\Phi} \tag{10}$$

$$b' = Is\frac{N^2}{k_z} e^{I\Phi}. \tag{11}$$

3 Direct numerical simulations: equations and numerical method

We solve the Navier-Stokes equations in the Boussinesq approximation for the deviation fields ($\vec{u}'$,b') from the balanced fields ($U(y,z), B(y,z)$). These equations are:

$$\frac{\partial u'}{\partial t} + (\vec{u}'.\nabla)u' + U\frac{\partial u'}{\partial x} + v'\frac{\partial U}{\partial y} + w'\frac{\partial U}{\partial z} = -\frac{1}{\rho_0}\frac{\partial p'}{\partial x} + fv' + \nu\nabla^2 u' \quad (12)$$

$$\frac{\partial v'}{\partial t} + (\vec{u}'.\nabla)v' + U\frac{\partial v'}{\partial x} = -\frac{1}{\rho_0}\frac{\partial p'}{\partial y} - fu' + \nu\nabla^2 v' \quad (13)$$

$$\frac{\partial w'}{\partial t} + (\vec{u}'.\nabla)w' + U\frac{\partial w'}{\partial x} = -\frac{1}{\rho_0}\frac{\partial p'}{\partial z} + b' + \nu\nabla^2 w' \quad (14)$$

$$\frac{\partial b'}{\partial t} + (\vec{u}'.\nabla)b' + U\frac{\partial b'}{\partial x} + v'\frac{\partial B}{\partial y} + w'\frac{\partial B}{\partial z} = \kappa\nabla^2 b' \quad (15)$$

$$\nabla.\mathbf{u} = 0, \quad (16)$$

where ρ_0 is a constant reference density and p' is the pressure deviation about the pressure field of the thermal balance state. A dimensional analysis can be briefly conducted to estimate the number of non dimensional parameters that govern the flow dynamics. Let U', k^{-1} and Ω^{-1} be the typical velocity, length and time scales of the wave motion; U_0, L_s and H_s be the typical velocity, horizontal length scale and vertical length scale of the shear flow. The wave motion also depends upon the parameters N, f, ν and κ. The flow dynamics therefore depend upon eight nondimensional parameters:

- For the wave field: $Fr_w = \dfrac{U'k}{N}$, the wave Froude number, $Re_w = \dfrac{U'}{k\nu}$, the wave Reynolds number, and the ratio Ω/N;
- For the shear flow: $Fr_s = \dfrac{U_0}{NH_s}$, the Froude number of the shear flow and the ratio $\dfrac{L_s}{H_s}$;
- For the wave-shear interaction: kH_s;
- For the medium: $\dfrac{f}{N}$ and $Pr = \dfrac{\nu}{\kappa}$, the Prandtl number.

Equations (12–16) are solved in a rectangular domain. The boundary conditions are periodic along the x and z directions and of free slip type along the y direction. These boundary conditions allow for the use of Fourier decomposition of the fields so that an efficient numerical algorithm, of the pseudo-spectral type, can be employed. Aliasing errors are removed using a standard truncation technique. Since we solve the equations of motion for the unbalanced components, the initial condition of the numerical code consists of the inertia-gravity wave packet only. These equations are integrated forward in time using a third-order Adams-Bashforth scheme.

We have performed several computations, which are listed in Table 1. The choice of the parameters was guided by the following point of view: the wave packet propagates into the current

in such a way that its intrinsic frequency increases because of the y-dependence of the shear flow. This means that the wave packet should be trapped in the neighbourhood of the $\Omega = N$ surface and, at least for $\beta = 0$, may break there. The purpose of our paper is to investigate the influence of the baroclinicity parameter β on the wave packet behaviour for $0 < \beta \leq 1$. Note that if Ω were decreasing during the propagation, the packet phase lines would flatten and the packet would reflect in the neighbourhood of the shear flow, according to the linear study of Öllers *et al.* (2003) [18].

4 Ray theory: equations and numerical method

4.1 Background

When a wave propagates in a moving fluid of velocity $\mathbf{U}$ and buoyancy B, a phase can be locally defined at any time if the period (Ω^{-1}) and wavelength (k^{-1}) of the wave are much smaller that the scale of the spatial and temporal gradients of the background fields. This is the basic assumption of the WKB approximation. The dispersion relation holds locally, with Ω, the intrinsic frequency of the wave, being simply shifted by the Doppler effect:

$$\omega = \Omega + \mathbf{k}.\mathbf{U}. \tag{17}$$

ω is the absolute frequency of the wave, namely the frequency measured in the frame of reference relative to which the fluid velocity is measured; in the present case, this absolute reference frame is the rotating frame of reference introduced above.

In this approximation, changes in the wave properties are controlled by the gradients of the ambient fields $\mathbf{U}$ and N and are predicted along a ray (see *f.i.* Olbers 1981 [17]). A ray is the trajectory of an observer moving with the absolute group velocity and is therefore defined by:

$$\frac{dx_i}{dt} = c_{gi} + U_i, \tag{18}$$

where $\mathbf{c}_g = \partial\Omega/\partial\mathbf{k}$ is the intrinsic group velocity, $\mathbf{c}_g + \mathbf{U}$ is the absolute group velocity and thus

$$\frac{d}{dt} = \frac{\partial}{\partial t} + (\mathbf{c}_g + \mathbf{U}).\nabla, \tag{19}$$

refers to changes seen by an observer moving with the absolute group velocity. We recall the expression of the group velocity :

$$\mathbf{c}_g = \left(\frac{\partial\Omega}{\partial k_i}\right) = \left(\frac{N^2-\Omega^2}{\Omega k^2}k_x, \frac{N^2-\Omega^2}{\Omega k^2}k_y, -\frac{\Omega^2-f^2}{\Omega k^2}k_z\right). \tag{20}$$

	Runs					
Parameters	1	2	3	4	5	6
(L_x, L_y, L_z)	$(4, 32, 10)$					
$(k_x, k_y, k_z)/2\pi$	$(1/4, 1/4, 1)$				$(1/4, 1/4, -1)$	
f	0.23					
N_0	1					
Pr	1					
U_0	-0.5					
y_s	5					
L_s	1	8	3	8		
β	0		0.5			1
H_s	–	–	10			
s_0	0.11					
y_p	-5					
z_p	5					
L_p	3					
H_p	1					
ν	10^{-4}					
$Fr_w(t=0)$	0.19					
$Re_w(t=0)$	44					
Fr_s	–	–	0.05			
Resolution	32x1201x128				32x601x256	32x1201x128

Table 1: Parameters of the direct numerical simulations. L_x, L_y and L_z are the size of the numerical domain along the x, y and z directions respectively. $Fr_w(t=0)$ and $Re_w(t=0)$ are the initial Froude and Reynolds numbers of the wave field and Fr_s is the (constant) Froude number of the shear flow. Non-specified values are those of the computation in the preceeding column. The number of wavelengths in the wave packet is $N_p^y = L_p.k_y/\pi = 1.5$ along the y direction and $N_p^z = H_p.k_z/\pi = 2$ along the z direction. All parameters are defined in section 2.

The wave vector is refracted by the gradients of the ambient fields $\mathbf{U}$ and N according to the equations (expressed along a ray):

$$\frac{dk_i}{dt} = -\frac{\partial \Omega}{\partial N}\frac{\partial N}{\partial x_i} - k_j \frac{\partial U_j}{\partial x_i}, \tag{21}$$

that is, in the present case, with $\mathbf{U} = (U(y,z), 0, 0)$ and $N(y,z)$

$$\frac{dk_x}{dt} = 0 \tag{22}$$

$$\frac{dk_y}{dt} = -\frac{\partial \Omega}{\partial N}\frac{\partial N}{\partial y} - k_x \frac{\partial U}{\partial y}, \tag{23}$$

$$\frac{dk_z}{dt} = -\frac{\partial \Omega}{\partial N}\frac{\partial N}{\partial z} - k_x \frac{\partial U}{\partial z}. \tag{24}$$

Since $\mathbf{U}$ and N do not vary in time, the absolute frequency of the wave packet remains constant along a ray. It follows that the intrinsic frequency varies along a ray according to (using (17)):

$$\begin{aligned} \frac{d\Omega}{dt} &= -k_j \frac{dU_j}{dt} - U_j \frac{dk_j}{dt}, \\ &= -k_x (c_{gy}\frac{\partial U}{\partial y} + c_{gz}\frac{\partial U}{\partial z}); \end{aligned} \tag{25}$$

the second equality makes use of the fact that $dk_x/dt = 0$.

Changes of the wave amplitude along a ray are inferred from the conservation of wave action. For any slowly varying background, the action $\mathcal{A} = E/\Omega$, where E is the wave energy, satisfies the conservation equation (Bretherton 1968 [3]):

$$\frac{\partial \mathcal{A}}{\partial t} + \nabla.[(\mathbf{c_g} + \mathbf{U})\mathcal{A}] = 0. \tag{26}$$

Equation (26) implies that the action contained in a small volume δV moving with the absolute group velocity is conserved, that is

$$\frac{d(\mathcal{A}\delta V)}{dt} = 0. \tag{27}$$

The form of the WKB theory we use is the approximation of geometrical optics but, for simplicity, the terminology *WKB approximation* will be employed throughout the paper.

4.2 A simple expression of wave-shear flow energy exchange

A simple estimate of the transfers of energy between the wave-induced motions and the shear flow is provided by the WKB approximation, in the linear regime. If one assumes that the wave is of small amplitude relative to the shear flow, the Boussinesq equations may be linearized about the thermal wind balance fields, leading to linear equations for the wave field. In the following, we assume that the mean flow is barotropic, that is, of the form $U(y)$. As is classical in linear stability analysis, the energetic term responsible for the interaction between the wave and the shear flow is $- < u'v'\partial U/\partial y >$, where $<>$ refers to some average (for instance over space). If we further assume that the WKB approximation is valid, namely the wave is locally plane and its properties vary much faster than the gradients of the basic fields, then $- < u'v' dU/dy >$ may be approximated by $- < u'v' > dU/dy$. Using relations (8) and (9), the latter term may be expressed as

$$- < u'v' > \frac{dU}{dy} = -\frac{s^2}{2}\frac{k_x k_y}{k_H^4}(\Omega^2 - f^2)\frac{dU}{dy}, \tag{28}$$

which can also written as, using definition (20) of the group velocity and relation (5):

$$- < u'v' > \frac{dU}{dy} = \frac{s^2}{2} \frac{\Omega}{k_z^2} \frac{k^2}{k_h^2} (-k_x c_{gy} \frac{dU}{dy}). \tag{29}$$

Using equation (25), one finally gets

$$- < u'v' \frac{dU}{dy} > \simeq - < u'v' > \frac{dU}{dy} = \frac{1}{4} \frac{s^2}{k_z^2} \frac{k^2}{k_h^2} \frac{d(\Omega^2)}{dt}. \tag{30}$$

If $d\Omega^2/dt > 0$, as in the present case, expression (30) implies that energy transfer occurs from the shear flow to the wave-induced motions.

4.3 Numerical method for solving the ray equations

We represent the spatial form of the wave packet using a set of rays whose initial points lie in a given plane $x =$ constant along the horizontal and vertical centre lines of the packet. We therefore need to initialize the wave vector and intrinsic frequency at each of these points. A wave packet will generally contain a distribution of wavenumbers and a distribution of frequencies. If the packet is a result of an initial disturbance at a given (absolute) frequency, that frequency will remain constant if the properties of the medium do not vary with time (which is the case we consider). With this in mind, we assume that the packet is characterized by a single absolute frequency. This implies that the absolute frequency is the same for all rays. We thus set the wave vector at the centre of the packet first and derive the absolute frequency there from the Doppler relation (17). Noting that k_x is constant for all rays, the initial values of k_y or k_z must vary across the packet as a result of the (weak) variations of U and N. At each point along the vertical centre line of the packet, k_z is evaluated by assuming that k_y has a constant value (equal to that at the packet centre). Similarly, along the horizontal centre line of the packet, k_y is computed by assuming that k_z keeps its value at the packet centre. The latter assumption has to be relaxed in a few cases where the implied value of $k_y^2 < 0$ if both ω and k_z are assumed constant. In such cases k_y is initialized to zero. Finally, the initial amplitude at each point is set according to (7).

Equations (18) and (21) are integrated numerically using the fourth order Runge-Kutta technique to find the position and wavenumber along the rays. We calculate the wave action, and hence the wave amplitude, from Eq. (27) by computing the change in volume of a small, initially regular tetrahedral element which moves along each ray. Thus for each distinct initial point of the wave packet we calculate the paths of four rays which form the vertices of the volume element. In presenting our results we ignore the three extra rays which serve only to allow us to calculate the change in action density. Typically we use an integration step length $h = 0.04$ and the tetrahedral element initially has length and height $r_0 = 0.1$. Results are qualitatively stable if these values are reduced as long as $h < r_0$.

5 Results

The configuration and set of parameters we have chosen ensure that $d\Omega/dt > 0$ as the wave packet enters the shear flow. This result is not obvious *a priori*. Indeed, the inequality $d\Omega/dt > 0$ is equivalent to

$$U_0 k_x k_z (N - f\frac{k_H}{k_z}) \left(\frac{k_y k_z}{k_H^2} \frac{H_s}{L_s} (1 - \tanh Y)(1 + \beta \sin Z) - 2\pi\beta \cos Z \right) < 0, \tag{31}$$

with $Z = 2\pi z/H_s$ and $Y = (y - y_s)/L_s$. In the present case, $U_0 < 0$, $k_x > 0$, $k_y > 0$ and $k_H \simeq k_y$ so that this inequality may be approximated as

$$(N - f\frac{k_y}{k_z}) \left(\frac{H_s}{L_s} (1 - \tanh Y)(1 + \beta \sin Z) - 2\pi\beta \frac{k_y}{k_z} \cos Z \right) > 0. \tag{32}$$

At the beginning of the computation, $\tanh Y \simeq -1$, $Z \simeq \pi$ and $k_y/k_z \simeq \pm 1/4$ so that the inequality becomes

$$\frac{H_s}{L_s} \pm \pi \frac{\beta}{4} > 0, \tag{33}$$

which is true for the range of parameters we consider.

The increase of the intrinsic frequency during propagation is illustrated for run 3 in Figure 1, using the WKB approximation. The baroclinicity parameter β is equal to 0.5 in this computation, implying that the trapping effect exists at all altitudes (*i.e.* $\partial U/\partial y \neq 0$, $\forall z$). The two terms responsible for the change in Ω, namely $-k_x c_{gy} \partial U/\partial y$ and $-k_x c_{gz} \partial U/\partial z$, are displayed along a central ray (minus the latter term, which is negative, is actually displayed for comparison). The same qualitative behaviour is observed at early times for all rays. Figure 1 shows that the propagation of the wave packet is indeed controlled by the y-dependence of the shear flow so that, as we shall see, Ω increases.

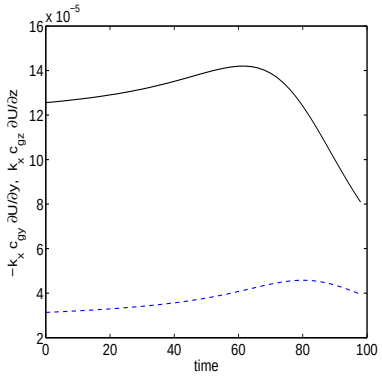

Figure 1: WKB predictions for run 3. The two terms responsible for the change in Ω are plotted versus time for a central ray. solid line: $-k_x c_{gy} \partial U/\partial y$; dotted line: $k_x c_{gz} \partial U/\partial z$.

5.1 Barotropic flow ($\beta = 0$)

When the baroclinicity parameter β is equal to 0, the shear flow is barotropic. WKB results are plotted for two such cases differing only in the width of the shear layer, namely run 1 (Figure 2a) and run 2 (Figure 2b). The surface $\Omega = N$, which is a vertical plane in this case, is displayed with a thick dashed line and a few illustrative contours of the velocity field are drawn using dotted lines.

Figures 2a and 2b show that, for either value of L_s, the rays eventually steepen and approach the $\Omega = N$ surface tangentially. The steepening may easily be accounted for. The intrinsic group velocity is perpendicular to $\vec{k}$ and parallel to the rays in the (y, z) plane (because the shear flow has no component in this plane). As the wave packet approaches the $\Omega = N$ surface, k_y increases because of the horizontal shear while k_x and k_z keep their initial value (see Eqs. (22) to (24)). Hence the intrinsic phase lines steepen and so do also the rays in the (y, z) plane. As a consequence, the intrinsic frequency along all rays increases with time (see relation (4)), which results in the trapping of the rays at the vertical plane defined by $\Omega = N$. All of the wave energy should accumulate at the trapping plane implying that, for a real wave field, breaking may occur there. Light grey regions on Figure 2b indicate points where the wave steepness exceeds 1, which would be associated with overturning for a real wave field (this region is also present on Figure 2a but hardly visible). As shown by Booker & Bretherton (1967) [2] and Wurtele *et al.* (1996) [22] however, the WKB predictions with respect to energetics differ from those for a real wave field using linear theory. Hence the light grey region cannot be expected to give a reliable prediction of where, and even whether, overturning will occur.

The ray paths indicated on Figures 2a and 2b give no indication of the speed of wave propagation. Since k_y increases monotonically and Ω approaches N, however, it is clear from Eq. (20) that all components of the group velocity approach zero, hence the propagation speed decreases strongly along the rays. It follows that in practice molecular effects, which are not taken into account in the ray equations, may cause a real wave to dissipate before overturning can occur.

DNS results for run 1 are displayed in Figure 3 through contours of the fluctuating buoyancy field. The behaviour just described is recovered: the wavelength along the y-direction decreases during propagation, resulting in a sudden increase of Ω at about $t = 80$ (figure 2c, further discussed below). As a consequence, the wave packet squashes onto the $\Omega = N$ trapping surface (figures 3b and 3c). The reduction of the wavelength in the $y-$direction is associated with an amplification of the fluctuating enstrophy at the packet centre E_Z, displayed in Figure 4. The packet centre is defined by the location $\mathbf{x}_0 = (x_0, y_0, z_0)$ where the fluctuating buoyancy field b' reaches a maximum

value. The enstrophy is half the vorticity squared and E_Z is therefore defined by

$$E_Z = \frac{1}{2}|(\nabla \wedge \vec{u}')(\mathbf{x}_0)|^2. \tag{34}$$

Figure 4 shows that E_Z increases to 8 times its initial value in run 1. However, E_Z first decreases by nearly a factor of 4, because of the dispersion of the wave packet. This dispersive effect is clearly manifested in the behaviour of the amplitude of the wave packet, as measured for instance by the maximum value of b' (figure 3d): the amplitude first decreases by a factor of 2. Interaction with the shear flow and trapping at the $\Omega = N$ surface next raises the amplitude of b' but the net increase from its initial value is by 20% only, a factor too small to result in wave breaking. Moreover, as the wave packet slows down along the trapping surface, molecular dissipation competes with the refractive focusing of wave energy, leading to a further decrease in maximum wave steepness. We find that the packet is eventually dissipated by molecular effects at the trapping plane.

Note that the fluctuating buoyancy field displayed in Figure 3 contains the wave field and the deviation of the shear flow from its balanced initial state, as a result of the interaction with the wave. The fact that there is no noticeable non-wavelike component suggests that the latter deviation is very small and that the displayed field may be assumed to belong to the wave packet only. This also implies that the shear flow is very weakly affected by the interaction.

Because the shear layer is very narrow in this run, the intrinsic frequency Ω stays constant until the packet reaches the trapping plane, then suddenly increases to a value around $0.8N/f$ (Figure 2c). Some time is needed, however, for the upper bound N/f to be reached. This behaviour is very likely due to the method we used to estimate Ω. We computed the intrinsic frequency at the packet centre from the equality $\Omega = \omega - k_x U(\mathbf{x}_0)$. Since, on the right hand side, only $\mathbf{x}_0$ is variable, discontinuities in Ω correspond to jumps in the location, $\mathbf{x}_0$, of maximum b'. The maximum jumps at $t \approx 80$ to a location closer to the $\Omega = N$ surface and slowly reaches that plane as the packet squashes.

The intrinsic frequency computed from the WKB approximation is also displayed in Figure 2c, for three rays. The general behaviour for each ray is close to that computed from DNS, namely Ω stays constant until the ray curves because of the change in background spatial gradients and increases to its upper bound N. The time at which Ω increases depends upon the ray location with respect to the trapping plane. Differences between WKB and DNS predictions in Figure 2c are thus principally a result of differences in definition of the packet centre. As far as the temporal evolution of Ω is concerned, we therefore conclude that ray trajectories are an appropriate model of the wave packet propagation in a barotropic shear flow.

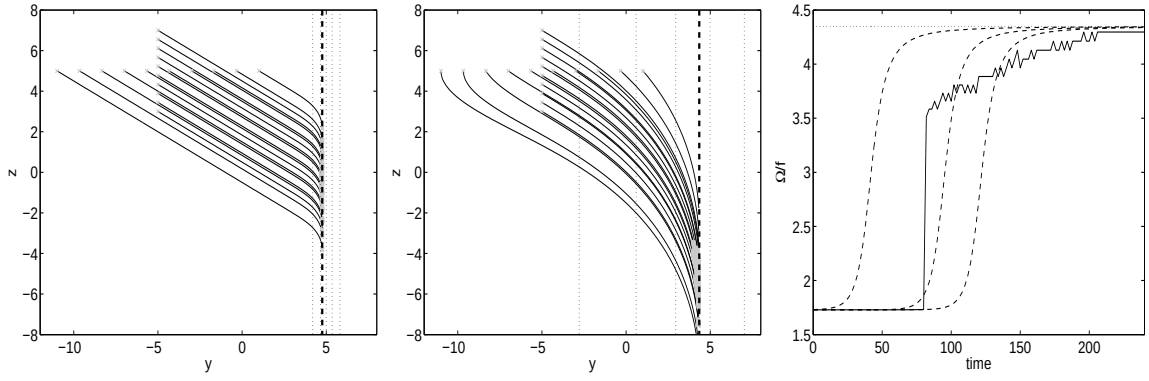

(a) (b) (c)

Figure 2: WKB predictions for run 1 (a) and run 2 (b). Trajectories of rays starting from the initial wave packet location for $t \leq 800$, in a vertical (y, z) plane. Light grey circles are plotted at each time the steepness along a given ray exceeds the value of 1. The thick dashed line marks the intersection of the $\Omega = N$ trapping surface with the (y, z) plane and dotted lines represent contours of the shear flow velocity in this plane. (c) Temporal evolution of the intrinsic frequency Ω of the wave packet normalized by the Coriolis frequency f for run 1; dashed line: WKB prediction for three rays of the packet; solid line: DNS result at the packet centre; dotted line: upper bound N/f.

5.2 Moderate baroclinicity ($\beta = 0.5$), strong horizontal shear

The parameter range for β being $[0, 1]$, we explored the baroclinic flow behaviour for $\beta = 0.5$ and $\beta = 1$, the latter value leading to quiet regions in the flow. In the present section, results for a relatively narrow shear layer are presented ($L_s = 3$), for $\beta = 0.5$ (run 3). The behaviour of the wave packet predicted by the WKB approximation and computed from direct numerical simulations for this run is displayed in Figures 5 and 6 respectively.

Figure 5a shows that k_y increases steadily as the wave propagates in the moving medium, reaching a value around 15 times its initial value at the end of the DNS at $t = 240$. The vertical component k_z increases at about the same rate as k_y for $100 < t < 200$ then decays to zero and becomes negative, implying that the rays become vertical then reflect.

Since the baroclinic parameter β is not zero, the surface $\Omega = N$ does not intersect the (y, z) plane in a straight vertical line. Instead, the surface flattens around the $z = z_n$ plane because U takes a minimum value there (Figure 5b). Therefore, the quasi-vertical rays meet the tilted $\Omega = N$ surface again in the $z = z_n$ region and reflect. The rays eventually become guided about the $z = z_n$ plane, between two sections of the $\Omega = N$ surface. One may wonder whether breaking will result since all of the wave energy should accumulate in this region.

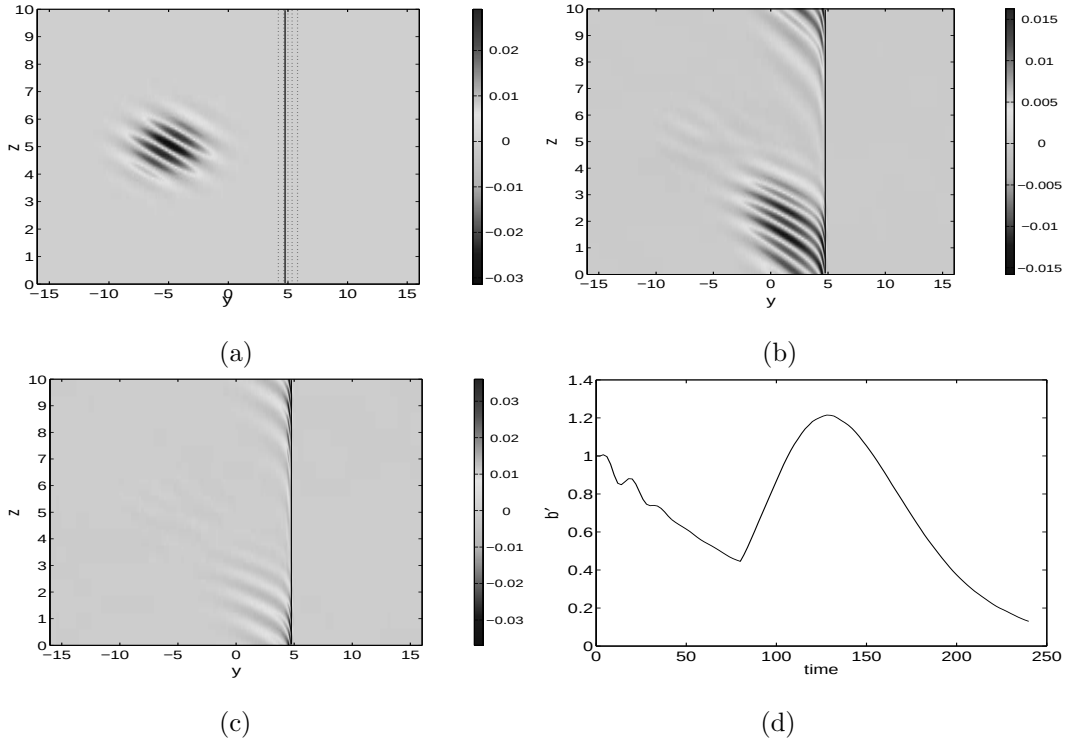

Figure 3: DNS results for run 1. (a) to (c) Constant contours of the fluctuating buoyancy field b' are plotted in a vertical (y, z) plane at successive times: (a) t=0 (a few contours of the shear flow velocity field are indicated with dotted lines), (b) t=84, (c) t=120. The vertical solid line marks the $\Omega = N$ trapping plane. Note the change in density scale between frames. (d) Value of the fluctuating buoyancy field b' at the packet centre, normalized by the value at $t = 0$, versus time.

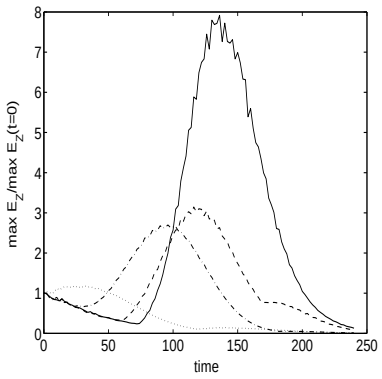

Figure 4: Enstrophy at the centre of the wave packet, E_Z, normalized by its initial value $E_Z(0)$, for the main runs discussed in the paper. Solid line: run 1; dashed line: run 3; dash-dotted line: run 4; dotted line: run 6.

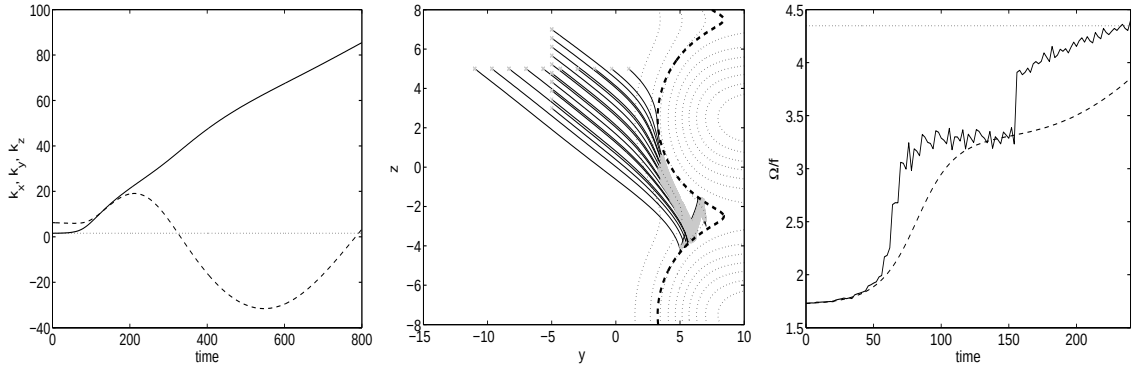

(a) (b) (c)

Figure 5: WKB predictions for run 3. (a) Components of the wave vector versus time along a central ray: k_x (dotted line), k_y (solid line) and k_z (dashed line). (b) Trajectories of rays starting from the initial wave packet location for $t \leq 800$, in a vertical plane. See caption of Figure 2 for the meaning of line types and symbols. (c) Intrinsic frequency versus time for the same ray as in (a), normalized by f (dashed line); Ω/f computed from DNS at the packet centre is displayed for comparison (solid line) as well as N/f (dotted line).

The numerical solution of the Boussinesq equations for run 3 displays a similar behaviour at early times. Constant contours of the fluctuating buoyancy field are displayed in Figure 6 for this run. As the wave packet propagates into the shear flow, the phase lines steepen and get trapped in the vicinity of the $\Omega = N$ surface (displayed with a solid line). The enstrophy at the packet centre (Figure 4) first decreases at the same rate as run 1 because of dispersion. It next increases while the wave packet progresses along the $\Omega = N$ surface. Because the shear U_0/L_s, which controls the interaction at early times, is lower in run 3 than in run 1, the maximum value reached by the enstrophy is lower as well. Also, because the position of the trapping surface is closer to the wave packet at initial time when L_s is larger, that maximum value is reached at an early time for run 3.

From $t \simeq 50$ (Figure 6b), the trapping surface guides the now vertically moving wave packet toward the $z = z_n$ region. The packet keeps progressing downwards with a very small group velocity and a very small wavelength along the y-direction (Figure 6c). When the packet again approaches the $\Omega = N$ surface, at $t \simeq 160$, the intrinsic frequency increases (Figure 5c) and reaches its upper bound, equal to N. The decay of the wavelength along the y direction makes the wave packet very sensitive to viscous effects and it starts dissipating (Figure 6d). This fact, along with the very small group velocity, explains why reflection is not observed in the DNS. Indeed, assuming that the WKB prediction is quantitatively reliable, Figure 5a shows that reflection would first occur for $t > 300$, that is $Nt/2\pi > 48$. In the DNS, the packet would have been totally dissipated by this time.

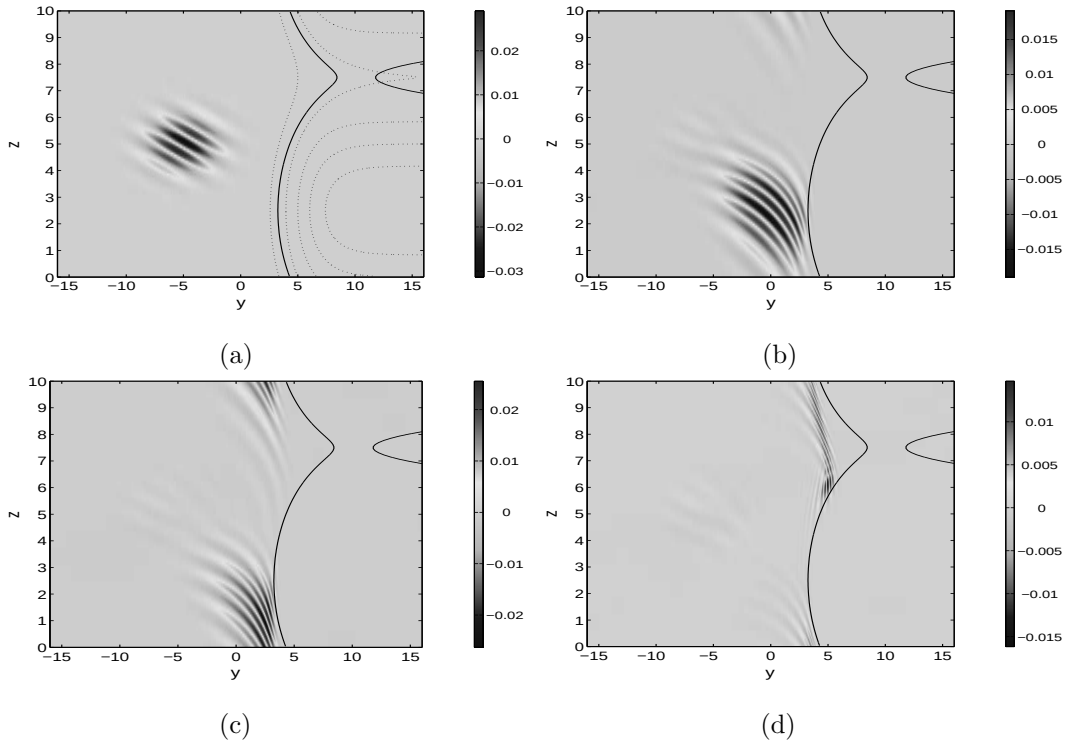

Figure 6: DNS results for run 3. Constant contours of the fluctuating buoyancy field b' are plotted in a vertical (y, z) plane at successive times: (a) t=0; (b) t=56, (c) t=84, (d) t=176. On frame (a), a few contours of the velocity field are plotted with dotted lines. The surface $\Omega = N$ is displayed with a solid line on all frames.

The intrinsic frequency Ω computed from the WKB approximation along a central ray is also displayed in Figure 5c. The agreement with the DNS behaviour is good up to $t \simeq 150$. However, the central ray has not yet reached the $\Omega = N$ surface at $t = 240$ (but is very close to it), which accounts for the discrepancy between the DNS result and the WKB prediction observed for $t > 150$.

5.3 Moderate baroclinicity ($\beta = 0.5$), weak horizontal shear

The penetration of the wave packet into the shear flow may be promoted by reducing the horizontal shear U_0/L_s. A consequence of this, however, is that a weaker amplification of the wave-induced velocity will occur. We have carried out two computations in which the parameter L_s is increased to a value of 5 and 8 while U_0 keeps the same value (equal to -0.5). The same qualitative behaviour is observed and only the results for the latter computation (run 4) are presented. Results from the WKB approximation are displayed in Figure 7 and those from DNS in Figure 8.

It is shown in Figure 7a that the $\Omega = N$ surface is no longer closed near the $z = z_n$ plane, thereby creating a region where the trapping effect due to the horizontal shear is so weak that the

rays penetrate into the shear flow. As before, all rays are first trapped by the $\Omega = N$ surface and steepen; they meet that surface again in the neighbourhood of the $z = z_n$ plane, because it has become almost horizontal, and reflect. In doing so, the rays become trapped between two sections of that surface, which form a guide, leading the rays to penetrate further into the shear flow. The components of the wave vector are displayed in Figure 7b for a central ray: k_y steadily increases up to 25 times its initial value while k_z oscillates about zero due to successive reflections of the ray.

Constant contours of the fluctuating buoyancy field computed from DNS are plotted at successive times for this run in Figure 8. The same behaviour as in the WKB approximation is observed again, up to the time the wave packet, which has steepened because of the trapping process, meets the $\Omega = N$ surface for the second time (panel d), in the neighbourhood of the $z = z_n$ plane. The horizontal shear is equal to at most $(1-\beta)U_0/L_s \simeq 0.03$ at this plane (we recall that U and $\partial U/\partial y$ take a minimum value there as z varies, for a constant y) while the wave shear is about $\simeq 0.45$ there. Hence, we expect the packet to further propagate into the shear flow in the neighbourhood of this plane because the horizontal shear of that flow is insignificant there.

Cross-hatching of the density field indicates a reflection of wave energy at this point, but the whole wave packet progresses so slowly that it is eventually dissipated before it can propagate away from the reflection region. Of course, this dissipation cannot be interpreted as an absorption at a critical level, since the intrinsic frequency of the wave packet is close to N in this region. More precisely, Figure 7c shows that, as in run 3, Ω increases toward its upper bound in two steps, as the wave packet approaches and moves away from the $\Omega = N$ surface. The WKB approximation is able to predict these two steps, very likely because the central ray has just reached the $\Omega = N$ surface at the end of the DNS. Hence, a good agreement is observed with DNS result during the whole duration of this run when Ω is considered. As expected from the discussion in the previous section, the enstrophy at the packet centre (displayed in Figure 4) reaches a smaller maximum value than in runs 1 and 3 (because U_0/L_s is smaller), but at an early time (because the trapping plane is closer), after decaying at the same rate through dispersion.

Figure 8 suggests that the wave packet, if propagating upwards instead of downwards from its initial location, would reach the $z = z_n$ plane without progressing along the trapping surface $\Omega = N$ and being slowed down. Thus, we performed the same computation as run 4, with the only difference that k_z was opposite signed (run 5, not shown). We found that the wave packet slowly penetrates into the shear flow by reflecting onto both sides of the $\Omega = N$ surface, as in the WKB prediction. Its amplitude has however decreased by a factor 100 by this time so that the induced motions within the guiding region are insignificant.

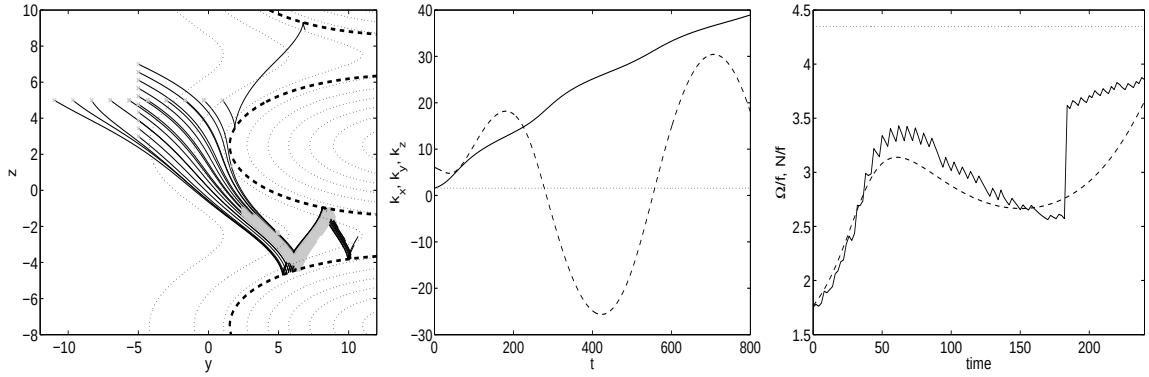

(a) (b) (c)

Figure 7: WKB predictions for run 4. (a) Trajectories of rays starting from the initial wave packet location for $t \leq 800$. See caption of Figure 2 for the meaning of line types and symbols. (b) Components of the wave vector for a central ray: k_x (dotted line), k_y (solid line) et k_z (dashed line) as a function of time. (c) Temporal evolution of the intrinsic frequency Ω of the wave packet normalized by the Coriolis frequency f; dashed line: WKB prediction for a central ray; solid line: DNS result at the packet centre; dotted line: upper bound N/f.

5.4 Strong baroclinicity ($\beta = 1$), weak horizontal shear

The previous computations have shown that the trapping of the wave packet by the horizontal shear of the balanced flow strongly slows down the progression of the packet. The packet, whose horizontal scale has decreased because of trapping, becomes subjected to molecular effects and is eventually dissipated. We showed that even a very weak trapping effect is enough to prevent the propagation of the wave packet. It follows that trapping has to be totally suppressed for the wave packet to penetrate into the shear flow. This situation is modelled in run 6: the baroclinity parameter β has been increased to a value of 1, implying that both the horizontal and vertical gradients of the mean flow (along with the mean flow itself) vanish at the $z = z_n$ planes. Also, the sign of the vertical component of the wave vector has been reversed to ensure that the wave packet propagates (upwards) toward the $z = z_n$ plane, without being trapped by and along the $\Omega = N$ surface. Results are displayed in Figure 9 for the WKB predictions and DNS results are reported in Figure 10.

The WKB theory predicts that, except for two rays, the wave packet should entirely penetrate into the shear flow. The vanishing of the gradients of the shear flow suppresses interaction with the latter flow and the amplitude of the wave packet is nearly unchanged; no grey region is indeed present on the ray trajectories.

A qualitative agreement with the WKB predictions is now observed over the whole duration

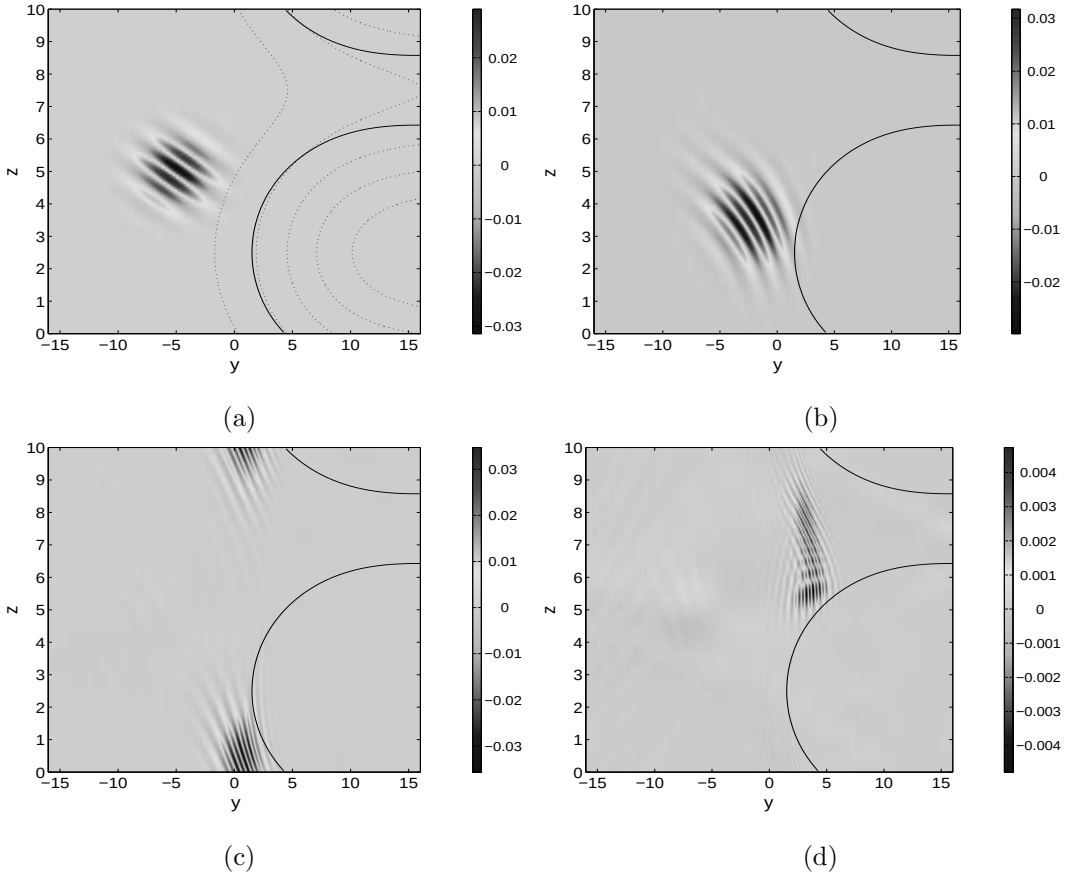

Figure 8: DNS results for run 4. Constant contours of the fluctuating buoyancy field b' are plotted in a vertical (y, z) plane at successive times: (a) t=0; (b) t=56, (c) t=84, (d) t=176. The surface $\Omega = N$ is displayed with a black line on all frames.

of the DNS (Figure 10). The wave packet is engulfed in the shear flow about the $z = z_n$ plane and propagates forward while being reflected onto the $\Omega = N$ surface. The absence of significant interaction with the shear flow is manifested in the temporal evolution of the enstrophy at the packet centre (Figure 4). Indeed, the enstrophy increases by 20% at most as the packet propagates toward the shear flow and then steadily decreases.

As opposed to all other runs, the intrinsic frequency at the packet centre initially decreases (Figure 9b). At $t \simeq 85$, when the packet first reflects onto the $\Omega = N$ surface, Ω suddenly grows to $\simeq 0.75N$ and then decreases, as the packet centre propagates toward the other side of the wave guide. The WKB approximation works surprinsingly well for $t < 85$ since it also predicts that Ω decays along the central ray. We recall that the theory is valid when the wavelength is much smaller than the thickness of the shear flow. In run 6, the wavelength is 2 along the $y-$direction (as indicated in Table 1) and does not decay during propagation (as opposed to the other runs), while $L_s = 8$. We are therefore led to conclude that a ratio of 1/4 meets the validity requirement

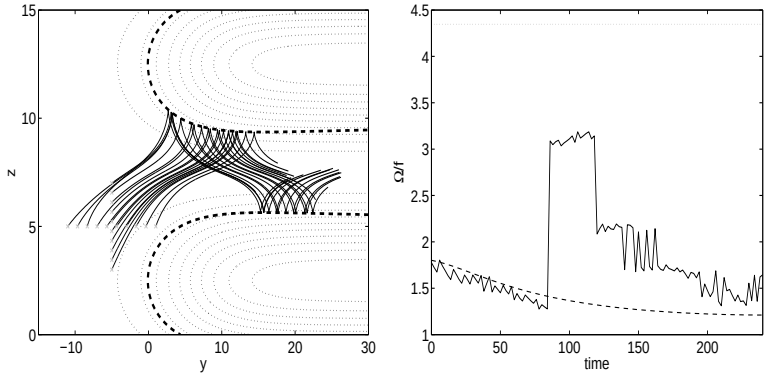

(a) (b)

Figure 9: WKB predictions for run 6. (a) Trajectories of rays starting from the initial wave packet location for $t \leq 800$. See caption of Figure 2 for the meaning of line types and symbols. (b) Temporal evolution of the intrinsic frequency Ω of the wave packet normalized by the Coriolis frequency f; dashed line: WKB prediction for a central ray; solid line: DNS result at the packet centre; dotted line: upper bound N/f.

of the theory. The discrepancy between DNS and WKB predictions for $t > 85$ again corresponds to a change in the location of maximum b' away from the position of the central ray, associated with an amplification of the buoyancy perturbation in the interference region around the reflection point.

6 Conclusions

The purpose of this paper was to investigate the interaction of an inertia-gravity wave packet with a unidirectional baroclinic shear flow $U(y, z)$, using the WKB approximation and three-dimensional direct numerical simulations. WKB predictions are remarkably well verified by the DNS at early times for all runs. The wave packet is trapped by the surface where the intrinsic frequency reaches its upper bound (*i.e.*, the local value of the Brunt-Väisälä frequency), moves along this surface with its nearly-vertical group velocity and reflects from this surface at, or near, locations where U takes a minimum value along the vertical direction (hence $\partial U/\partial z = 0$ at this location). Significant deviations from WKB predictions were found when the wave packet became strongly trapped. The wavelength along the direction of inhomogeneity (y and z), and hence also the group velocity, decreases during propagation. Molecular dissipation therefore has time to affect the small scales, competing with the refractive focusing of wave energy. In our example situation, the packet is eventually dissipated close to the first reflection point. Only when the shear flow vanishes locally along with its derivatives is the packet able to penetrate into the shear flow. But almost no interaction with the shear flow occurs in the latter case so that, except for momentum deposition

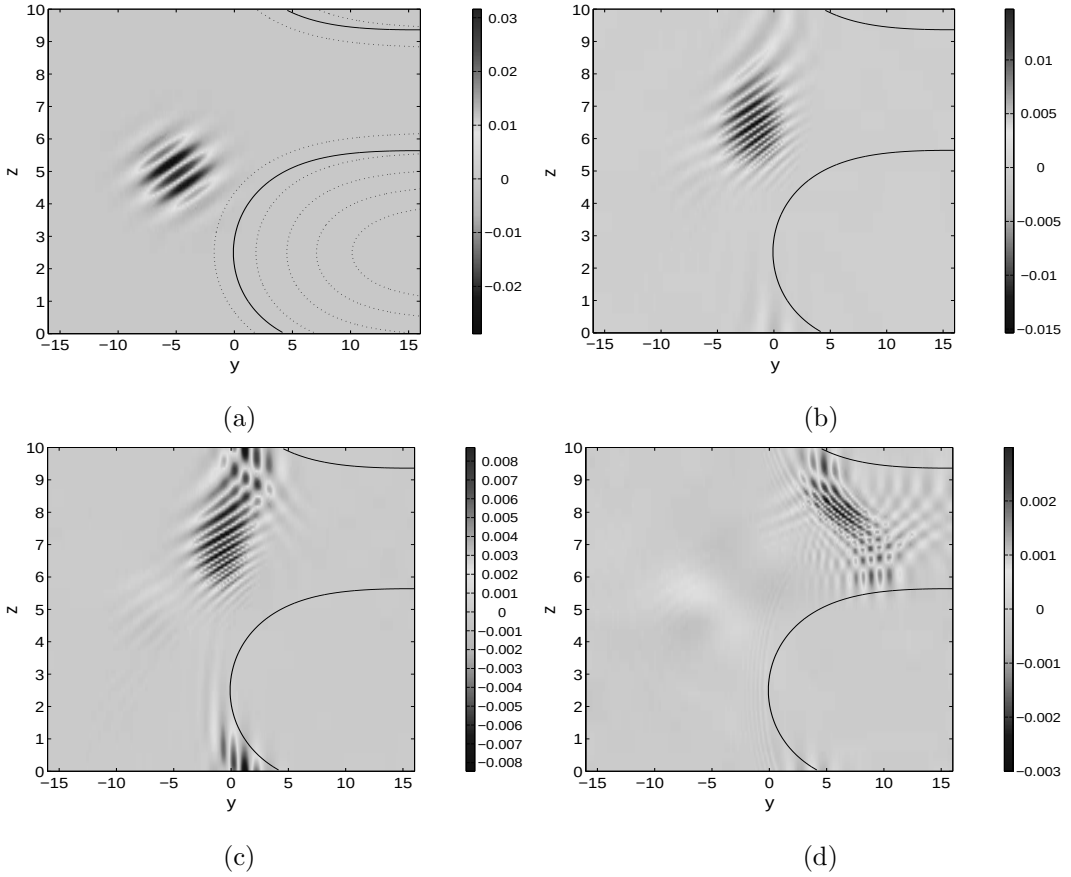

Figure 10: DNS results for run 6. Constant contours of the fluctuating buoyancy field b' are plotted in a vertical (y, z) plane at successive times: (a) t=0 (a few contours of the shear flow velocity are displayed with dotted lines); (b) t=56, (c) t=84, (d) t=204. The surface $\Omega = N$ is displayed with a solid line on all frames.

through dissipative effects, the wave packet is not expected to induce any modification of the ambient flow.

An important feature of the DNS results is the rapid dispersion of the wave packet. Dispersion and, to a lesser extent, dissipation counteract the focusing of wave energy and effectively prevent overturning, and consequently tracer mixing. In our simulations the packet is initially defined as a single-wavenumber perturbation modulated by a Gaussian envelope, which is equivalent to specifying a distribution of wavenumbers. The precise influence of the form and length of the packet on the interaction is difficult to assess. In additional simulations, not shown here, we have found that similar packets propagating in unsheared flow and initially only one or two wavelengths long in one direction can elongate by dispersion by up to 60% in only 4 wave periods, an order of magnitude more than packets containing 5 wavelengths (Edwards & Staquet 2004 [6]). Longer packets, which approximate more closely a single wavenumber, may therefore exhibit less dispersion

but unfortunately require considerably more computing time. Wavenumber interactions could counteract dispersion even in short packets, allowing them to propagate with little change of form but exact solutions corresponding to such behaviour are known only in certain special cases (Thorpe 2002 [20]). According to Badulin (2004, private communication) the earlier theoretical analysis of Erokhin & Sagdeev 1985 ([7], [8] papers in Russian) already showed that the amplitude of an internal gravity wave packet strongly attenuates due to dispersion, thereby making the trapping process less dramatic than for plasma waves for instance, which disperse less because their group velocity behaves as $1/k^{\alpha}$, with $\alpha < 1$.

The study we have conducted is somewhat academic but geophysical implication can still be inferred. Thus, because the waves are unable to cross the shear flow barrier and are dissipated in its near neighbourhood, we expect weaker inertia-gravity wave activity to be found inside large-scale geophysical vortices than outside. Of course, more work is necessary to quantify this conjecture.

Further work is currently being performed to address cases where stronger interaction occurs.

Acknowledgements

We are grateful to S.I. Badulin and S.A. Thorpe for fruitful discussions. NRE was supported by the Service Hydrographique et Oceanographique de la Marine (SHOM/CMO) under Contracts 00.87.040 and 01.87.075. Computations were performed on the national computer centre IDRIS.

References

[1] Badulin SI, Shrira VI 1993. On the irreversibility of internal-wave dynamics due to wave trapping by mean flow inhomogeneities. Part 1. Local analysis. *J. Fluid Mech.* 251:21–53

[2] Booker JR, Bretherton FP 1967. The critical layer for internal gravity waves in a shear flow. *J. Fluid Mech.* 27:513–39

[3] Bretherton FP 1968. Propagation in slowly varying wave guides. *Proc. Roy. Soc. London* A302:555–77.

[4] Bretherton FP 1966. The propagation of groups of internal gravity waves in a shear flow. *Quart. J. Roy. Met. Soc.* 92:466–80

[5] Brown SN, Stewartson K 1982. On the nonlinear reflection of a gravity wave at a critical level. Part 3. *J.Fluid Mech.* **115**, 231–250.

[6] Edwards NR, Staquet C 2004. In preparation.

[7] Erokhin NS, Sagdeev RZ 1985a. On the theory of anomalous focusing of internal waves in a two-dimensional nonuniform fluid. part 1. A stationary problem. *Morsk. Gidrofiz. J.*, **2** 15-27.

[8] Erokhin NS, Sagdeev RZ 1985b. On the theory of anomalous focusing of internal waves in a horizontally inhomogeneous fluid. Part 2. Precise solution of the two-dimensional problem with respect to viscosity and non stationarity. *Morsk. Gidrofiz. J.*, **4** 3-10.

[9] Gill AE 1985. Atmosphere-Ocean dynamics. *International Geophysics Series*, **vol. 30**, Academic Press.

[10] Ivanov YA, Morozov YG 1974. Deformation of internal gravity waves by a stream with horizontal shear. *Okeanologie*, **14**, 457–61

[11] Jones WJ 1967. Propagation of internal gravity waves in fluids with shear flow and rotation. J. Fluid Mech. **30**, 439–49

[12] Jones WJ 1968. Reflexion and stability of waves in stably stratified fluids with shear flow: a numerical study . J. Fluid Mech. **34**, 609–24

[13] Jones WJ 1969. Ray tracing for internal gravity waves. *J. Geophys. Research*, **74**-8, 2028–33

[14] LeBlond PH, Mysak LA 1978. Waves in the Ocean. Elsevier Oceanography Series 20, Elsevier Pub.

[15] Michalke A 1964. On the inviscid instability of the hyperbolictangent velocity profile, *J. Fluid Mechanics.*, **19**, 543–56

[16] Moulin F, Flor JB 2004. Experimental study on the wave-breaking and mixing properties of a tall vortex. Submited to *Dyn. Atmos. Oceans*

[17] Olbers DJ 1981. The propagation of internal waves in a geostrophic current. *J. Phys. Oceanogr.* 11:1224–33

[18] Öllers MC, Kamp LPJ, Lott F, Van Velthoven PFJ, Kelder HM, Sluijter FW 2003. Propagation properties of inertia-gravity waves through a barotropic shear layer and application to the Antarctic polar vortex. *Quart. J. Roy. Met. Soc.*, **129**-B, 2495.

[19] Staquet C, Huerre G 2002. On transport across a barotropic shear flow by breaking inertia-gravity waves. *Phys. Fluids*, **14**(6), 1993–2006.

[20] Thorpe S.A. 2002. On the dispersion of pairs of internal inertial gravity waves. *J. Marine Research*, **60** (3): 461-76

[21] Winters KB, D'Asaro EA 1994. Three-dimensional wave instability near a critical level, *J. Fluid Mechanics.*, **272**, 255–84

[22] Wurtele MG, Datta A, Sharman RD 1996. The propagation of gravity-inertia waves and lee waves under a critical level. *J. Atmos. Sciences*, **53**-11, 1505.